

# Flowfield Calculation of Electrothermal Pulsed Plasma Thrusters for Osaka Institute of Technology Small Satellite

IEPC-2009-253

*Presented at the 31st International Electric Propulsion Conference,  
University of Michigan • Ann Arbor, Michigan • USA  
September 20 – 24, 2009*

Yusuke Ishii<sup>1</sup>, Hiroki Takagi<sup>2</sup> and Hirokazu Tahara<sup>3</sup>  
*Osaka Institute of Technology, Asahi-Ku, Osaka, 535-8585, Japan*

**Abstract:** The Project of Osaka Institute of Technology Electric-Rocket-Engine onboard Small Space Ship (PROITERES) was started at Osaka Institute of Technology. In PROITERES, a small satellite with electrothermal pulsed plasma thrusters (PPTs) will be launched in 2010. The main mission is powered flight of small satellite by electric thruster. An unsteady numerical simulation was carried out to investigate physical phenomena in the discharge system including plasma and discharge electric circuit and to predict performance characteristics for electrothermal PPTs. The Mach number intensively increased downstream from the discharge cavity exit; that is, the supersonic flow was established in the nozzle cathode. Both the calculated impulse bit and mass shot were higher than the measured ones with a discharge energy per one shot of 2.4 J/s for the satellite although with 14.6 J/s the calculated results agreed well with the measured ones.

## Nomenclature

$C$	= electric capacitance
$e$	= internal energy or electron charge
$E_i$	= corresponding voltage of ionization
$j$	= current density
$J$	= discharge current
$k$	= Boltzmann factor or heat conductivity
$L$	= electric inductance
$m$	= particle mass
$M$	= momentum flux
$n$	= number density
$p$	= pressure
$q$	= heat flux
$Q$	= Joule heat
$r$	= radial coordinate
$R$	= electric resistance
$t$	= time
$T$	= temperature
$V$	= velocity
$z$	= axial coordinate
$\alpha$	= degree of ionization
$\varphi$	= particle number flux

---

<sup>1</sup> Graduate Student, and Department of Mechanical Engineering.

<sup>2</sup> Graduate Student, and Department of Mechanical Engineering.

<sup>3</sup> Professor, Department of Mechanical Engineering, and tahara@med.oit.ac.jp.

$\rho$	=	density
$\rho_p$	=	electric resistance
$\sigma_{e-n}$	=	cross-section of electron-neutral collision
$\Gamma$	=	mass flux
$\Theta$	=	temperature
$\ln A$	=	Coulomb logarithm

### Subscript

$0$	=	initial
$e$	=	electron
$i$	=	ion
$n$	=	neutral
$r$	=	radial direction
$s$	=	surface
$z$	=	axial direction

## I. Introduction

THE Project of Osaka Institute of Technology Electric-Rocket-Engine onboard Small Space ship (PROITERES), as shown in Fig.1, was started at Osaka Institute of Technology.<sup>1</sup> In PROITERES, a small satellite with electrothermal pulsed plasma thrusters (PPTs) will be launched in 2010. The main mission is powered flight of small satellite by electric thruster. The orbit raising will be carried out by the PPTs.

Pulsed plasma thrusters are expected to be used as a thruster for a small satellite. The PPT has some features superior to other kinds of electric propulsion. It has no sealing part, simple structure and high reliability, which are benefits of using a solid propellant, mainly Teflon<sup>®</sup> (poly-tetrafluoroethylene: PTFE). However, performances of PPTs are generally low compared with other electric thrusters.

At Osaka Institute of Technology, the PPT has been studied since 2003 in order to understand physical phenomena and improve thrust performances with both experiments and numerical simulations. We mainly studied electrothermal-acceleration-type PPTs, which generally had higher thrust-to-power ratios (impulse bit per unit initial energy stored in capacitors) and higher thrust efficiencies than electromagnetic-acceleration-type PPTs. Although the electrothermal PPT has lower specific impulse than the electromagnetic PPT, the low specific impulse is not a significant problem as long as the PPT uses solid propellant, because there is no tank nor valve for liquid or gas propellant which would be a large weight proportion of a thruster system.

In the present study, an unsteady numerical simulation is carried out to examine physical phenomena in the PPT discharge system including plasma and discharge electric circuit and to predict performance characteristics for the small satellite.

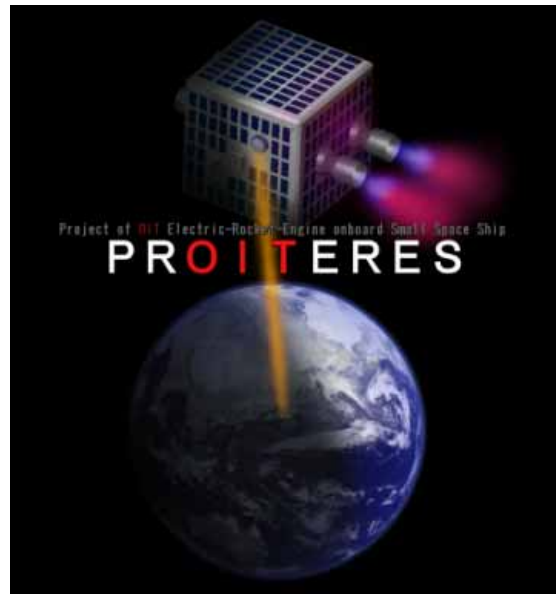
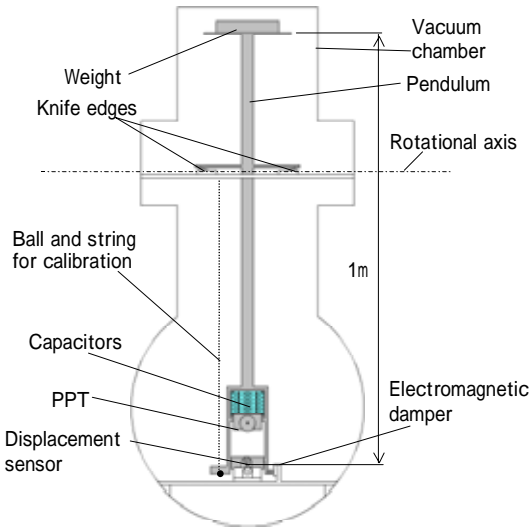


**Figure 1. Illustration of powered flight of Osaka Institute of Technology small space ship by electric rocket engine.**

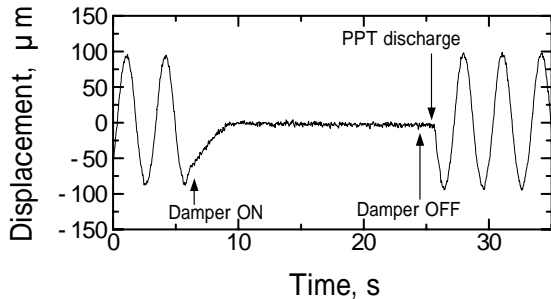
## II. Thrust Measurement System

Figure 2 shows a thrust stand in a vacuum chamber for precise measurement of an impulse bit. The PPT and capacitors are mounted on the pendulum, which rotates around fulcrums of two knife edges without friction. The displacement of the pendulum is detected by an eddy-current-type gap sensor (non-contacting micro-displacement meter) near the PPT, which resolution is about  $\pm 0.5 \mu\text{m}$ . The electromagnetic damper is used to suppress mechanical noises and to decrease quickly the amplitude for the next measurement after firing the PPT. It is useful for a sensitive thrust stand because it is non-contacting. The damper consists of a permanent magnet fixed to the

pendulum and two coils fixed to the supporting stand. The control circuit differentiates the output voltage of the displacement sensor and supplies the current proportional to the differentiated voltage to the coil. Accordingly, the damper works as a viscosity resistor. The damper is turned off just before firing the PPT for measurements without damping, and turned on after the measurement to prepare for the next measurement. Figure 3 shows a typical signal of displacement in measurement of impulse bit. Sensitiveness of the thrust stand is variable by changing the weight mounted on the top of the pendulum as shown in Fig. 4. A calibration of the thrust stand is carried out by collisions



**Figure 2. Thrust stand.**



**Figure 3. Typical signal of displacement in measurement of impulse bit.**

of balls to the pendulum with various balls from various distances corresponding 15-1400  $\mu\text{Ns}$ .

Figure 5 shows a vacuum chamber 1.25 m in length and 0.6 m in inner diameter, which is evacuated using a turbo-molecular pump with a pumping speed of 3,000 l/s. The pressure is kept below  $1.0 \times 10^{-2}$  Pa during PPT operation.

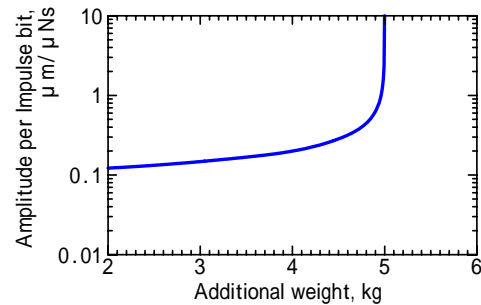


**Figure 4. Sensitiveness of thrust stand vs top weight.**



**Figure 5. Vacuum chamber.**

### III. Numerical Calculation

#### A. Calculation model

An unsteady numerical simulation is carried out to investigate physical phenomena in the PPT discharge system including plasma and discharge electric circuit and to predict performance characteristics.<sup>2-5</sup> Figure 6 shows the calculation model of the PPT system. The calculation simultaneously simulates unsteady phenomena of discharge in the circuit, heat transfer to the PTFE, heat conduction inside the PTFE, ablation from the PTFE surface and plasma flow. The calculation domain of the discharge chamber, as shown in Fig. 7, in the nozzle cathode and in the cylindrical cavity made of PTFE (Teflon). The length and diameter of the cavity are changed considering operational conditions.

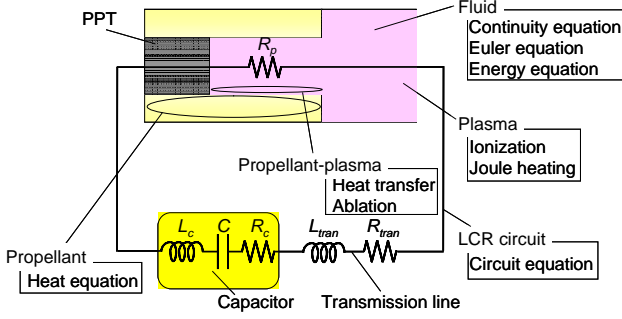


**Figure 6. Calculation model for PPT system.**

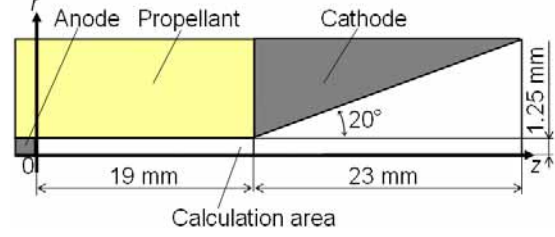


**Figure 7. Calculation domain.**

## B. Governing equations

Axisymmetric two-dimensional unsteady flowfield equations, conservation equations of mass, momentum and energy, are written as follows:

Mass:

$$\frac{\partial}{\partial t} \rho + \frac{\partial}{\partial r} M_r + \frac{\partial}{\partial z} M_z = -\frac{1}{r} M_r \quad (1)$$

Momentum (Euler Eqs.):

*r*-direction:

$$\frac{\partial}{\partial t} M_r + \frac{\partial}{\partial r} \left[ \frac{M_r^2}{\rho} + p \right] + \frac{\partial}{\partial z} \left[ \frac{M_r M_z}{\rho} \right] = -\frac{1}{r} \frac{M_r^2}{\rho} \quad (2)$$

*z*-direction:

$$\frac{\partial}{\partial t} M_z + \frac{\partial}{\partial r} \left[ \frac{M_r M_z}{\rho} \right] + \frac{\partial}{\partial z} \left[ \frac{M_z^2}{\rho} + p \right] = -\frac{1}{r} \frac{M_r M_z}{\rho} \quad (3)$$

Energy:

$$\frac{\partial}{\partial t} e + \frac{\partial}{\partial r} \left[ \frac{M_r}{\rho} (e + p) \right] + \frac{\partial}{\partial z} \left[ \frac{M_z}{\rho} (e + p) \right] = -\frac{1}{r} \frac{M_r}{\rho} (e + p) + Q_j \quad (4)$$

where  $\rho$ ,  $p$ , and  $e$  are density, pressure and internal energy of flow, respectively, and  $M_r$  and  $M_z$  are momentum fluxes of radial and axial directions, respectively.  $Q_j$  is Joule heat.

Ionization equilibrium is assumed as follows:

Saha Eq.:

$$\frac{\alpha^2}{1 - \alpha^2} = 2.6 \frac{(kT)^{5/2} (2\pi m_e)^{3/2}}{ph^3} + \exp\left(-\frac{qE_i}{kT}\right) \quad (5)$$

where  $\alpha$  and  $T$  are degree of ionization and temperature of flow, respectively, and  $E_i$  is corresponding voltage of ionization, in which the average ionization voltage of PTFE decomposed atoms (carbon and hydrogen etc.) are used.

The Joule heat is written as follows:

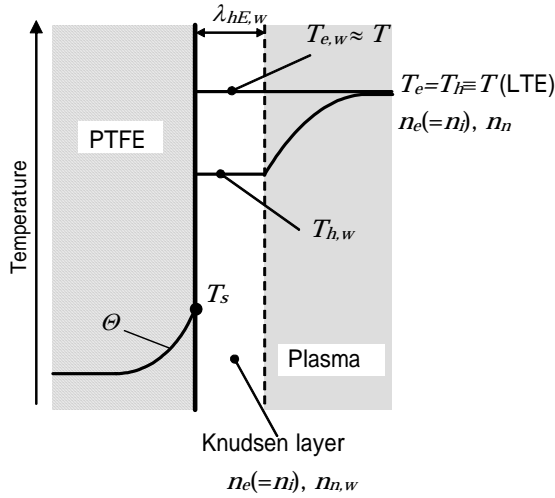
$$Q_j = \rho_p j^2 \quad (6)$$

$$\rho_p = \frac{\ln \Lambda}{1.53 \times 10^{-2} T^{3/2}} + \frac{m_e}{n_e e^2} \sigma_{e-n} n_n \left( \frac{3kT}{m_e} \right)^{1/2}$$

$$\ln \Lambda = \ln[12\pi m_e (\epsilon_0 kT / e^2 n_e)^{3/2}]$$

where  $\rho_p$  is electric resistance corresponding electron-ion and electron-neutral collisions, in which  $n_e$  and  $n_n$  are densities of electron and neutral, respectively, and  $j$  is current density in axial direction.

Figure 8 shows the model of heat fluxes from plasma to PTFE surface in the cavity, and their heat fluxes and the interaction are written as follows:



Heat convection:

$$q_{h,conv} = \alpha_i (\varphi_i + \varphi_n) \cdot 2k(T_{h,w} - T_s) \quad (7)$$

Heat conduction:

$$q_{h,cond} = k \frac{\partial T_{h,w}}{\partial r} \quad (8)$$

Interaction Eq.:

$$q_{h,conv} = q_{h,cond} \quad (9)$$

**Figure 8. Heat transfer inside PTFE.**

where  $\varphi_i$  and  $\varphi_n$  are particle number fluxes of ion and neutral, respectively, to PTFE surface.

In evaporation of PTFE on the cavity wall, we uses the following equations:  
Langmuir's law:

$$\Gamma = \left( \frac{m_n}{2\pi k T_s} \right)^{1/2} p_{vap} \quad (10)$$

$$p_{vap} = p_c \exp(-T_c / T_s)$$

$$( p_c = 1.84 \times 10^{15} \text{ Pa}, T_c = 20815 \text{ K} )$$

Evaporation heat flux:

$$q_{ab} = \frac{\Gamma}{m_n} \cdot 2kT_s \quad (11)$$

where  $\Gamma$  and  $q_{ab}$  are mass and heat fluxes, respectively, from PTFE surface, and  $p_{va}$  and  $T_s$  are evaporation pressure and PTFE surface temperature, respectively.

In heat conduction inside the PTFE block, the heat conduction equation and the boundary condition are written as follows:

$$\frac{\partial \Theta}{\partial t} = \frac{\kappa}{\rho_{PTFE} C_p} \left( \frac{\partial^2 \Theta}{\partial r'^2} + \frac{1}{r'} \frac{\partial \Theta}{\partial r'} + \frac{\partial^2 \Theta}{\partial z^2} \right) \quad (12)$$

$$\kappa \frac{\partial \Theta}{\partial r} \Big|_{r=0} = (Q_{conv} - Q_{ab})$$

where  $\Theta$  is temperature inside the PTFE.

Finally, we close the equation system by using the following electric circuit equation:  
From Fig. 6:

$$(L_{tran} + L_c) \ddot{Q} + (R_{tran} + R_c + R_p) \dot{Q} + \frac{Q}{C} = 0 \quad (13)$$

$$J = -\dot{Q}$$

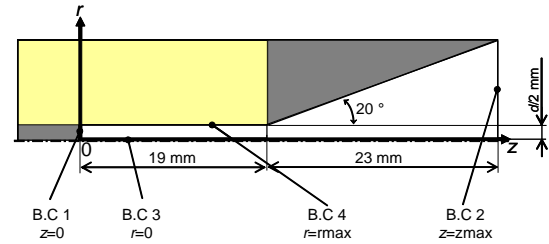
Initial condition:

$$Q_0 = CV_0$$

### C. Calculation procedure and conditions

After all equations were normalized, the flowfield equations are numerically solved by TVD-MacCormack scheme and average of Roe. In the calculation process, the electric circuit equation is solved by Runge-Kutta method, and the axial current density is obtained. The boundary conditions shown in Fig. 9 are assumed. For calculation start, a very low density plasma is distributed just before the calculation. The calculation grid sizes are 0.5 mm in axial direction and 0.025 mm in radial direction, and the time step is  $10^{-9}$  s.

The experimental and calculation conditions are shown in Tables 1 and 2. The discharge energies per one shot are 14.6 and 2.4 J/shot; that is, the capacitance is changed. Accordingly, the length and diameter of discharge cavity are changed to find preferable cavity configuration. The discharge energy per one shot is lowered to 2.4 J/shot for the small satellite.



	$\rho$	$M_r$	$M_z$	$e$
B.C 1	$\frac{\partial \rho}{\partial z} = 0$	$\frac{\partial M_r}{\partial z} = 0$	$M_z = 0$	$\frac{\partial e}{\partial z} = 0$
B.C 2	$\frac{\partial \rho}{\partial z} = 0$	$\frac{\partial M_r}{\partial z} = 0$	$\frac{\partial M_z}{\partial z} = 0$	$\frac{\partial e}{\partial z} = 0$
B.C 3	$\frac{\partial \rho}{\partial r} = 0$	$M_r = 0$	$\frac{\partial M_z}{\partial r} = 0$	$\frac{\partial e}{\partial r} = 0$
B.C 4	$\Delta \rho_r = \rho_{ab}$	$M_r = \Gamma$	$\frac{\partial M_z}{\partial r} = 0$	$\Delta e_r = Q_{ab} - Q_{conv}$

Figure 9. Boundary conditions.

**Table 1. Experimental and calculating condition with discharge energy per one shot of 14.6 J/s.**

Discharge chamber	Length, mm	19
	Diameter, mm	2.5, 3.0, 3.5
Nozzle	Length, mm	23
	Half angle, degree	20
Charging voltage, V		1800
Capacitance, $\mu\text{F}$		9.0

**Table 2. Experimental and calculating condition with discharge energy per one shot of 2.4 J/s.**

Discharge chamber	Length, mm	9.0
	Diameter, mm	1.0, 1.5, 2.0, 2.5
Nozzle	Length, mm	23
	Half angle, degree	20
Charging voltage, V		1800
Capacitance, $\mu\text{F}$		1.5

#### IV. Results and Discussion

##### A. Calculation results

Figure 10 shows typical measured and calculated discharge current signals with a discharge energy of 14.6 J/s. The calculated current signal agrees with the measured one.

Figure 11 shows the calculated Mach number distribution just after 3  $\mu\text{s}$  from the discharge start with 14.6 J/s. The Mach number intensively increases downstream from  $z=19\text{mm}$ ; that is, the supersonic flow is established. At  $z=35\text{mm}$ , the Mach number drastically decreases downstream, resulting from structure of shock wave.

Figure 12 shows the calculated time histories of normalized density, thrust, ablated mass and Joule heating at  $r=1.25\text{mm}$  and  $z=9.5\text{mm}$  with 14.6 J/s. The Joule heating begins at approximately 1  $\mu\text{s}$ ; it is completed by 7  $\mu\text{s}$ , and the ablation from the PTFE surface relays about 1-2  $\mu\text{s}$  from the Joule heating. The density gradually increases from about 2  $\mu\text{s}$ ; it has a peak at 9  $\mu\text{s}$ , and then it decreases. The thrust gradually increases from 4  $\mu\text{s}$ , and it has a peak at 13  $\mu\text{s}$ . Accordingly, the thrust is generated until over 20  $\mu\text{s}$ . Thrust generation is expected to be related to increase in density.

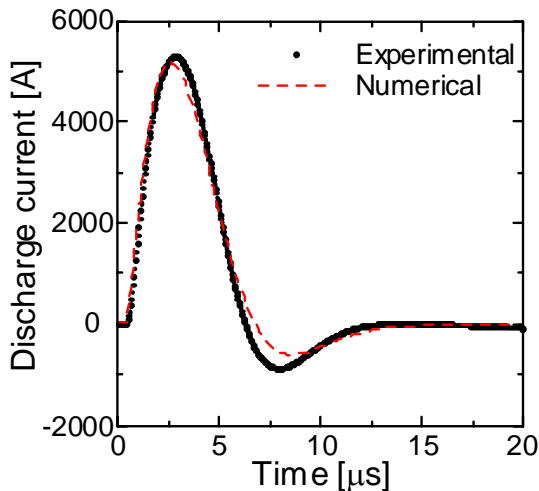


Figure 10. Discharge current signal.

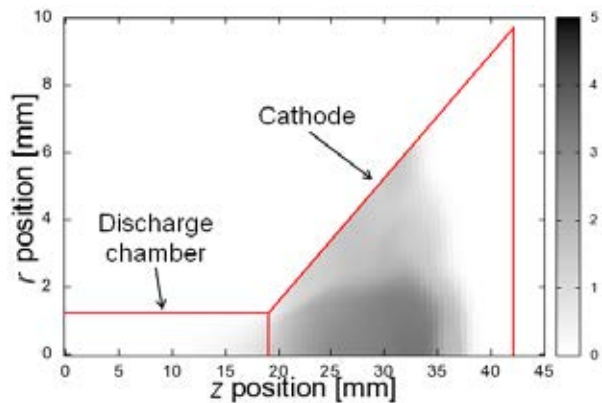


Figure 11. Mach number distribution.

Figure 13 shows axial the calculated distributions of normalized density, velocity and ablation flux near the cavity wall just after 10  $\mu\text{s}$  from the discharge start with 14.6 J/s. The velocity linearly increases from the upstream end to the cavity exit although the density gradually decreases. An axial decrease in ablation flux is due to the axial decrease in density because of lowering heat convection to the PTFE surface.

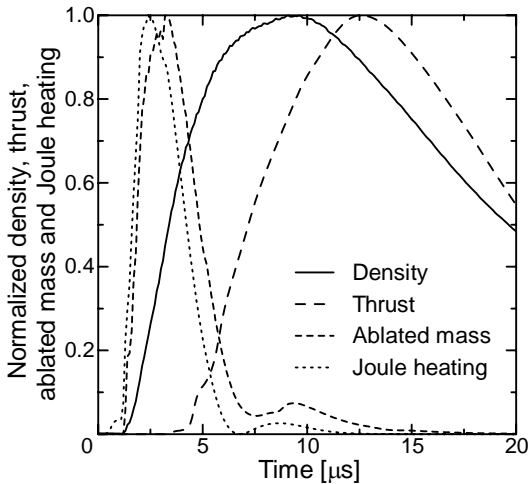


Figure 12. Normalized density, thrust, Joule heating and ablated mass.

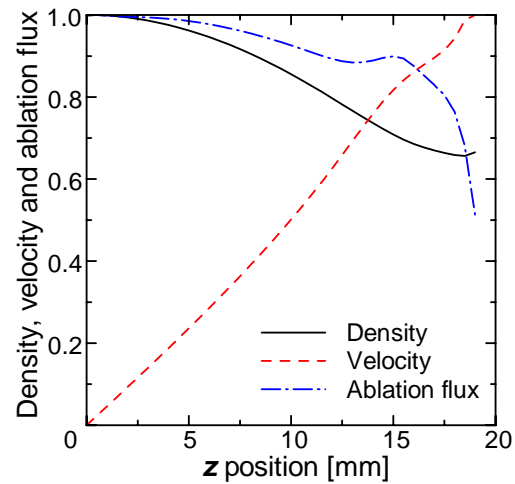
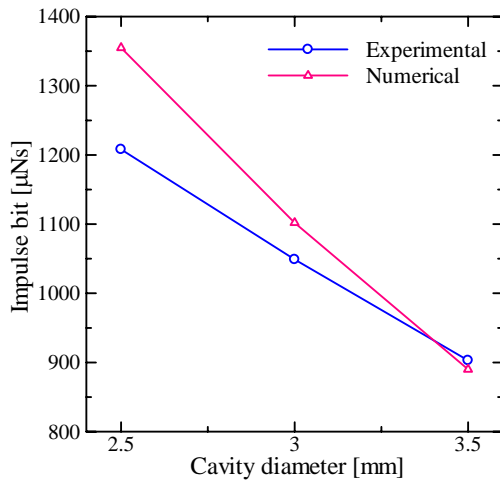


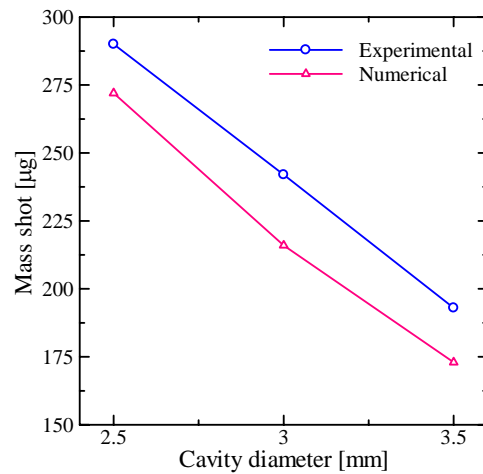
Figure 13. Normalized density, velocity, and ablation flux.

### B. Comparisons with experimental results

Figure 14 shows measured and calculated impulse bit and mass shot dependent on cavity diameter with a constant cavity length of 19 mm with a discharge energy per one shot of 14.6 J/s. Both the impulse bit and the mass shot decrease with increasing cavity diameter regardless of calculation and experiment. The calculated impulse bit roughly agrees with the measured one although with a small diameter of 2.5 mm it is slightly higher. On the other hand, the calculated mass shot agrees with the measured one, and its error is within 10 % although it is lower with all cavity diameters.



(a)



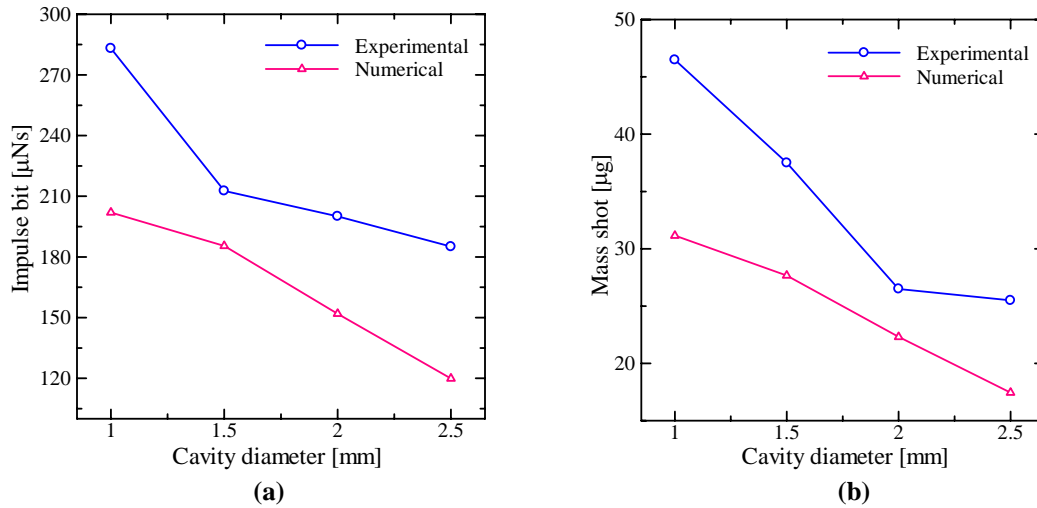
(b)

Figure 14. Experimental and numerical results with discharge energy per one shot of 14.6 J/s: a) impulse bit, b) mass shot.

Figure 15 shows measured and calculated impulse bit and mass shot dependent on cavity diameter with a constant cavity length of 9 mm with a discharge energy per one shot of 2.4 J/s. Both the calculated impulse bit and



mass shot are higher than the measured ones, and their errors are above 20 % with all cavity diameters. We need to improve the calculation model with cases with low discharge energies.



**Figure 15. Experimental and numerical results with discharge energy per one shot of 2.4 J/s: a) impulse bit, b) mass shot.**

## V. Conclusions

An unsteady numerical simulation was carried out to investigate physical phenomena in the PPT discharge system including plasma and discharge electric circuit and to predict performance characteristics for the small satellite.

The Mach number intensively increased downstream from  $z=19\text{mm}$  of the discharge cavity exit; that is, the supersonic flow was established. At  $z=35\text{mm}$  in the nozzle cathode, the Mach number drastically decreased downstream, resulting from structure of shock wave.

In a discharge cavity, the Joule heating and the ablation from the PTFE surface were completed up to  $10\ \mu\text{s}$  just after the discharge start. After the intensive ablation, the thrust was generated until over  $20\ \mu\text{s}$ . The velocity linearly increased from the upstream end to the discharge cavity exit although the density gradually decreased. An axial decrease in ablation flux was due to the axial decrease in density.

With a discharge energy per one shot of  $14.6\ \text{J/s}$ , both the impulse bit and the mass shot decreased with increasing cavity diameter regardless of calculation and experiment. The calculated impulse bit roughly agreed with the measured one. On the other hand, the calculated mass shot agreed well with the measured one.

With  $2.4\ \text{J/s}$ , both the calculated impulse bit and mass shot were higher than the measured ones, and their errors were above 20 % with all cavity diameters. We need to improve the calculation model with cases with low discharge energies for the small satellite

## References

- <sup>1</sup>Takagi, H., Ishii, Y., Yamamoto, T., and Tahara, H., "Research and Development of Electrothermal Pulsed Plasma Thrusters for Project of Osaka Institute of Technology Electric-Rocket-Engine onboard Small Space Ship (PROITERES)," *26th International Symposium on Space Technology and Science*, Hamamatsu, Paper No. ISTS2008-b-54p, June 2008.
- <sup>2</sup>Ishii, Y., Takagi, H., Yamamoto, T., and Tahara, H., "Flowfield Calculation of Electrothermal Pulsed Plasma Thrusters onboard the Osaka Institute of Technology Small Satellite," *27th International Symposium on Space Technology and Science*, Tsukuba, Paper No. ISTS2009-b-15, July 2009.
- <sup>3</sup>Edamitsu, T., Tahara, H., "Performance Measurement and Flowfield Calculation of an Electrothermal Pulsed Plasma Thruster with a Propellant Feeding Mechanism," *29th International Electric Propulsion Conference*, Paper IEPC-05-105, Nov. 2005.
- <sup>4</sup>Edamitsu, T., and Tahara, H., "Experimental and Numerical Study of an Electrothermal Pulsed Plasma Thruster for Small Satellite," *Vacuum*, Vol. 80, 2006, pp. 1223-1228.
- <sup>5</sup>Keider, M., Boyd, I.D., and Beilis, I.I., "Model of an Electrothermal Pulsed Plasma Thruster," *IEEE Transactions on Plasma Science*, Vol. 28, No. 2, 2000, pp. 376-385.